Oxygen and Carbon Dioxide Permeability of EAA/PEO Blends and Microlayers

V. V. Pethe,[1] H. P. Wang,[1] A. Hiltner,[1] E. Baer,[1] B. D. Freeman[2]

[1]*Department of Macromolecular Science and Engineering, Case Western Reserve University, Cleveland, Ohio 44106-7202*
[2]*Department of Chemical Engineering, Center for Energy and Environmental Resources, The University of Texas at Austin, Austin, Texas 78758*

Received 20 November 2007; accepted 26 December 2007
DOI 10.1002/app.28193
Published online 17 July 2008 in Wiley InterScience (www.interscience.wiley.com).

ABSTRACT: The goal of this study was to broaden the spectrum of gas permeability and selectivity characteristics of poly(ethylene-*co*-acrylic acid) (EAA) by combining it with poly(ethylene oxide) (PEO), which has a high selectivity for CO_2. To obtain films that differed substantially in their solid state morphologies, EAA was combined with PEO as melt blends and as coextruded films with many alternating, continuous microlayers of EAA and PEO. The solid state structure and thermal behavior were characterized and the permeability to O_2 and CO_2 was measured at 23°C. When the PEO was dispersed as small domains, the particles were too numerous for most of them to contain a heterogeneity that was sufficiently active to nucleate crystallization at the normal T_c. The rubbery, amorphous nature of the PEO domains enhanced the gas permeability of the melt blends. In contrast, the constituent polymers maintained the bulk properties in 5–20 μm-thick microlayers. The series model accurately described the gas transport properties of microlayered films. Comparison of blends and microlayers revealed that the high CO_2 selectivity of PEO was most effectively captured when the PEO phase was continuous, as in the microlayers or in the cocontinuous 50/50 (wt/wt) melt blend. © 2008 Wiley Periodicals, Inc. J Appl Polym Sci 110: 1411–1419, 2008

Key words: polyethylene oxide; blends; microlayers; oxygen permeability; carbon dioxide permeability

INTRODUCTION

Polyethylene is widely used in film applications due to its low cost and excellent processibility. It would be a candidate for additional packaging applications if a broader spectrum of gas permeability and selectivity characteristics were achieved. A useful strategy for controlling structure–property relationships and improving the performance of polymeric materials involves blending with suitable functional constituents. Poly(ethylene oxide) (PEO) possesses an unusually high selectivity for CO_2 over nonpolar gases such as O_2, N_2, and H_2.[1,2] Whereas the CO_2 permeability of a polyethlene film is about 4× the O_2 permeability, this value rises to 16× for PEO. This characteristic makes PEO attractive for gas separation and atmosphere control applications.[3]

Polyethylene and PEO are incompatible in melt blends. One approach that has been used to combine polyethylene and PEO is the synthesis of copolymers containing poly(ethylene oxide) side chains grafted to poly(ethy1ene-*co*-acrylic acid).[4] It also appears that the presence of carboxyl groups on the polyethylene improves the compatibility. When PEO was blended with polyethylene under conditions that oxidized the polyethylene, much better dispersion was achieved.[5] Acid functionality can be introduced in a much more controlled manner with poly(ethylene-*co*-acrylic acid) (EAA) copolymers. It can be imagined that, depending of the concentration of acrylic acid groups, blends of EAA with PEO could range from immiscible to completely miscible.[6]

In the present study, we sought to broaden the spectrum of gas permeability and selectivity characteristics of ethylene-based polymers by combining EAA with PEO. To obtain films that differed substantially in their solid state morphology, EAA was combined with PEO as melt blends and as coextruded films with many alternating, continuous microlayers of EAA and PEO. The solid state structure and thermal properties were characterized and the permeability to O_2 and CO_2 was measured.

MATERIALS AND METHODS

Poly(ethylene oxide) (PEO) with M_w of 200 kg/mol was purchased in powder form from Sigma Aldrich (St. Louis, MO) and was also obtained in pellet form. An ethylene acrylic acid copolymer (EAA) with 9.7 wt % acrylic acid (Primacor1430) was

Correspondence to: A. Hiltner (ahiltner@case.edu).
Contract grant sponsor: NSF Center for Layered Polymeric Systems; contract grant number: DMR-0423914.

© 2008 Wiley Periodicals, Inc.

obtained from The Dow Chemical Company (Midland, MI) in the form of pellets.

Before blending, the PEO powder and the EAA were dried *in vacuo* at 40°C for 24 h. The constituents were blended in a Haake (Karlsruhe, Germany) minilab twin screw microcompounder. The screw diameter was 1/8'' with a L/D ratio of 24:1. Typically, material was mixed in the microcompounder for about 3 min at 190°C. Blends with (EAA/PEO) 90/10, 80/20, 70/30, and 50/50 (wt/wt) were prepared. In addition, EAA and PEO were processed under the same conditions. The controls and blends were compression molded at 190°C and solidified by circulating cold water through the compression molder. The molded films were ~ 250 μm in thickness and measured about 10 cm × 9 cm.

Films with 17 alternating PEO and EAA layers with EAA outer layers were fabricated using the layer multiplication process described previously.[7,8] The PEO and the EAA were dried thoroughly before extrusion. The extruder temperatures of 150°C for PEO and 160°C for EAA were chosen to ensure matching viscosities when the polymer melts were combined in the feedblock. The layered melt was spread in a 6'' film die. The temperature of the layer multipliers and film die was 160°C. Rapid quenching on a chill roll equipped with an air knife froze the melt morphology. The feed ratio was controlled with metering pumps to obtain microlayer films with (EAA/PEO) 80/20, 70/30, 60/40, 50/50, and 40/60 (vol/vol). The nominal layer thicknesses were calculated from the number of layers, the feed ratio, and the film thickness. In addition, coextrusions were carried out under the same conditions with either EAA or PEO in both extruders. These films were used as controls. The films were stored at ambient temperature in desiccators to prevent moisture absorption.

The density of EAA films was measured with a density gradient column constructed from an aqueous solution of propanol at 23°C according to ASTM-D 1505 Method B. The column was calibrated with glass floats of known density. Small pieces of film (~ 25 mm^2) were placed in the column and allowed to equilibrate for 30 min before the measurements were taken. The density of EAA compression molded films was 0.9405 g cm^{-3} and the density of EAA microlayered films was 0.9341 g cm^{-3}.

Because of the water solubility of PEO, the film density was determined by hydrostatic weighing using a Mettler Toledo balance (Model XS205, Greifensee, Switzerland) and a density determination kit.[1] In this method, the film density ρ is calculated as

$$\rho = \frac{M_A}{M_A - M_L}\rho_o \tag{1}$$

where M_A and M_L are the film weights in air and in an auxiliary liquid, respectively, and ρ_o is the density of the auxiliary liquid. It is reported that PEO is insoluble in isooctane,[1] which was used as the auxiliary liquid. Iso-octane 99.8% pure was obtained from Sigma Aldrich (St. Louis, MO). The isooctane had density 0.692 g cm^{-3}. The film weight in isooctane was recorded as quickly as possible to reduce the possibility of swelling.

For atomic force microscopy (AFM), the films were embedded in 5-min epoxy and cured overnight at 23°C. Cured specimens were sectioned perpendicular to the plane of the film at −75°C with a cryo-ultramicrotome (MT6000-XL from RMC, Tucson, AZ). The surfaces were examined at ambient conditions using the tapping mode of the Nanoscope IIIa MultiMode scanning probe microscope (Digital Instruments, Santa Barbara, CA). The probe radius was 5–10 nm. Phase and height images were recorded simultaneously. Phase images most clearly revealed the blend morphology.

Thermal analysis (DSC) was conducted with a Perkin–Elmer DSC-7 (Boston, MA) calibrated with indium and tin. Scans were performed under nitrogen at a heating/cooling rate 10°C min^{-1} over the temperature range from −60 to 140°C.

The oxygen flux was measured with a Mocon Ox-Tran 2/20 (Minneapolis, MN) at 0% RH and at a temperature of 23°C or 11°C. The CO_2 flux was measured at 0% RH and 23°C with a Mocon Permatran-C 4/40. To prevent the steady-state flux through the thin, highly permeable films from exceeding the detector range, the O_2 or CO_2 pressure in the permeant stream was reduced to 0.02 atm by mixing with nitrogen.[9] The instruments were calibrated with National Institute of Standards and Technology certified Mylar film of known O_2 and CO_2 transport characteristics. The specimens were carefully conditioned in the instrument, as described previously.[10] The O_2 permeability $P(O_2)$ and the CO_2 pereambility $P(CO_2)$ were calculated from the steady state flux J as

$$P = J\frac{l}{p} \tag{2}$$

where l is the film thickness and p is the permeant gas pressure. The selectivity was estimated as $P(CO_2)/P(O_2)$.

When possible, the nonsteady state flux $J(t)$ was recorded from which the diffusivity D was determined. To obtain D and to accurately determine P the data were fit to the solution of Fick's second law with appropriate boundary conditions

$$J(t) = \frac{Pp}{l}\left[1 + 2\sum_{n=1}^{\infty}(-1)^n \exp\left(-\frac{D\pi^2 n^2 t}{l^2}\right)\right] \tag{3}$$

As indicated previously,[10] the error in determining the two fitting parameters P/L and D/L^2 was esti-

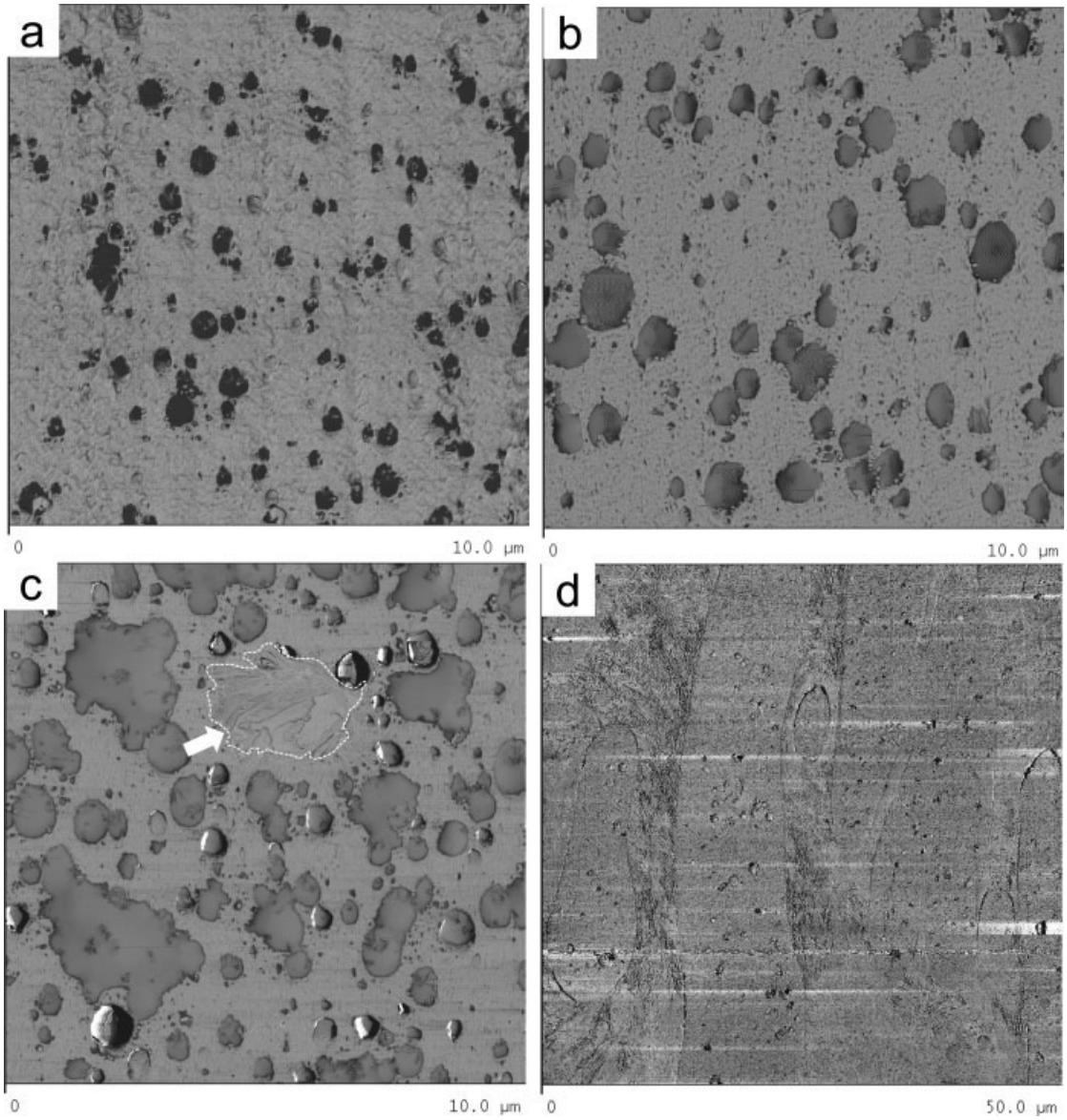

Figure 1 AFM phase images of compression molded EAA/PEO blends: (a) 90/10 blend; (b) 80/20 blend; (c) 70/30 blend; and (d) 50/50 blend. Note the change in scale of (d). The arrow points to the outline of a crystalline PEO domain.

mated not to exceed 2%. Therefore, the accuracy of P and D was determined mainly by the accuracy of the average thickness measurement. The thickness was measured at nine locations on the film with a micrometer and the average was used in the calculations. The solubility S was obtained from the relationship $S = P/D$.

RESULTS AND DISCUSSION

Characterization of EAA/PEO blends

The AFM images of the 90/10, 80/20, and 70/30 (EAA/PEO) blends show that the PEO was dispersed as particles in a continuous EAA matrix, Figure 1(a–c). In contrast, the morphology of the 50/50 blend consisted of large cocontinuous domains, Figure 1(d). The dispersed PEO domains of the 90/10, 80/20, and 70/30 (EAA/PEO) blends were generally spherical except in the 70/30 blend where coalescence produced a number of larger, irregular domains. The mean diameters of PEO domains were determined from image analysis to be about 0.30 μm, 0.37 μm, and 0.59 μm, for 90/10, 80/20, and 70/30 (EAA/PEO) blends, respectively. Coalescence produced a broad domain size distribution in the 70/30 blend.

Heating and cooling thermograms of compression molded PEO, EAA and the blends are compared in Figure 2. The heating scan of PEO exhibited a sharp melting endotherm with peak melting temperature T_m at 65°C. The cooling scan revealed a sharp crys-

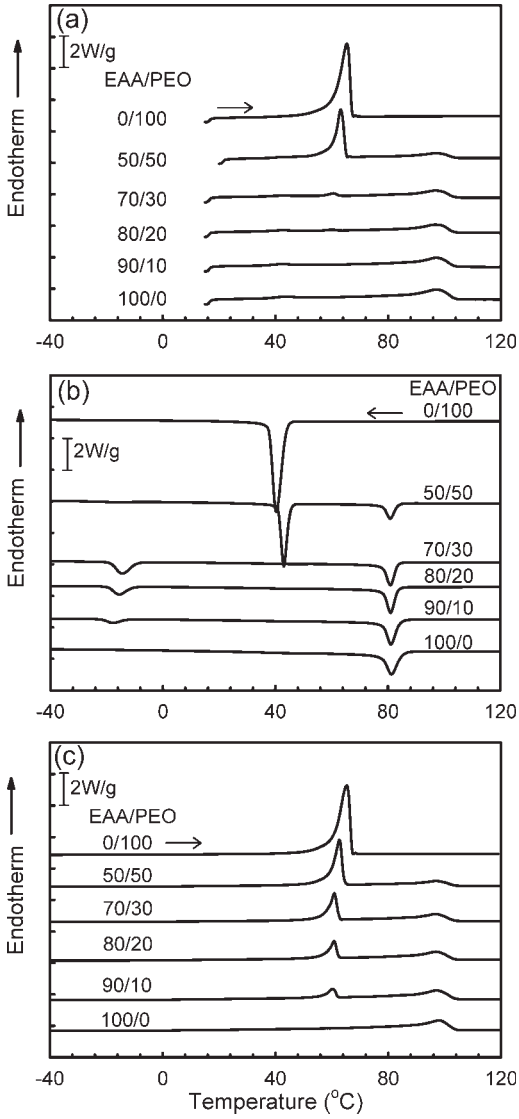

Figure 2 Thermograms of compression molded EAA/PEO blends at a heating/cooling rate of 10°C min^{-1}: (a) First heating thermograms beginning at 20°C; (b) subsequent cooling thermograms; and (c) second heating thermograms.

tallization exotherm with peak temperature T_c at 40°C. The crystallinity calculated from ΔH_m was 77% using a ΔH° value of 197 J g^{-1}.[11] The EAA exhibited a broad melting endotherm at 97°C and a sharp crystallization exotherm at 81°C. The crystallinity calculated from ΔH_m was 29% using a ΔH° value of 290 J g^{-1}.[11] Small endotherms at 40°C were attributed to room temperature annealing.

All the blends exhibited a melting peak for the EAA constituent at 97°C in the heating thermograms, Figure 2(a). Correspondence of the melting temperature with that of EAA, and close proportionality between ΔH_m and the blend composition were consistent with immiscibility of the blend constituents. The 50/50 blend showed a sharp melting peak for the PEO constituent at 63°C, slightly lower than the T_m of PEO at 65°C. The measured ΔH_m was close to that predicted from the blend composition. However, the PEO constituent in the 90/10, 80/20, and 70/30 (EAA/PEO) blends exhibited only a very small melting peak at about 60°C. Moreover, ΔH_m was substantially lower than expected based on the blend composition. Thus, it appeared that the PEO constituent was not able to crystallize in these blends.

The cooling thermograms in Figure 2(b) showed that the EAA constituent in the blends crystallized at 80°C with ΔH_c close to that predicted from the composition. The PEO constituent in the 50/50 blend crystallized at 43°C. For the 50/50 blend, ΔH_c was close to that predicted from the composition. However, the PEO constituent in the 90/10, 80/20, and 70/30 (EAA/PEO) blends did not crystallize until the blend was cooled to about −15°C. When the PEO did crystallize, ΔH_c was close to that predicted from the blend composition. Upon subsequent heating, the PEO constituent melted at the normal temperature of about 60°C, Figure 2(c). Close adherence to the additive melting and crystallization behavior was consistent with immiscibility of the constituent polymers. For subsequent analysis, the blend composition (wt/wt) was determined from the measured ΔH_m values in the second DSC heating thermogram. When the composition (vol/vol) was required, the conversion was performed using the measured densities, Table I.

It is now apparent why the compression molded 90/10, 80/20, and 70/30 (EAA/PEO) blends did not exhibit a melting endotherm for the PEO constituent. When the PEO was dispersed as small domains, the particles were too numerous for most of them to contain a heterogeneity that was sufficiently active to nucleate crystallization at the normal T_c. Hence, most of the particles crystallized at a much larger undercooling by fractionated crystallization or by homogeneous nucleation. Most studies put the temperature for homogeneous nucleation of PEO between −20 and −40°C.[12–16] Because the lowest temperature that the compression molded blends experienced during solidification in the compression molder was about + 15°C, well above the crystallization temperature of −15°C, the PEO particles did not crystallize, but remained indefinitely in the rubbery, amorphous state. The T_g of PEO is reported to be about −60°C.[17] In contrast, only a few heterogeneities were required to nucleate crystallization of the large, cocontinuous domains of the 50/50 blend.

The rubbery nature of the PEO domains in 90/10, 80/20, and 70/30 (EAA/PEO) blends was also inferred from the AFM phase images. Good contrast between the phases was achieved due to the large modulus difference between the rubbery PEO

TABLE I
Composition and Oxygen Permeability of EAA/PEO Blends

Target composition EAA/PEO (wt/wt)	Measured composition from DSC EAA/PEO (wt/wt)	Calculated composition from density EAA/PEO (vol/vol)	Density (g/cm^3)	$P(O_2)$ (barrer)	$P(CO_2)$ (barrer)	$\frac{P(CO_2)}{P(O_2)}$
100/0	100/0	100/0	0.9405 ± 0.0001	1.77 ± 0.02	5.49 ± 0.02	3.10
90/10	91/9	93/7	0.958 ± 0.001	2.27 ± 0.06	7.38 ± 0.06	3.25
80/20	83/17	86/14	0.977 ± 0.001	2.60 ± 0.05	9.36 ± 0.05	3.60
70/30	73/27	78/22	0.992 ± 0.001	2.69 ± 0.02	11.3 ± 0.02	4.20
50/50	55/45	61/39	1.064 ± 0.002	0.52 ± 0.03	4.09 ± 0.03	7.86
0/100	0/100	0/100	1.219 ± 0.004	0.40 ± 0.05	6.71 ± 0.53	16.8

domains and the crystalline EAA matrix. The low modulus of the rubbery PEO domains caused them to appear dark in the higher modulus, crystalline EAA matrix. If the PEO crystallized, the phases were more difficult to distinguish due to the similarity in the moduli. Occasionally, a larger PEO domain in the 70/30 (EAA/PEO) blend was brighter than the others and difficult to distinguish from the EAA matrix [arrow in Fig. 1(c)]. These domains had crystallized. They were responsible for the small PEO melting endotherm in the thermogram of the 70/30 blend [see Fig. 2(a)]. Similarity in the moduli of crystallized PEO and EAA in the 50/50 blend made it difficult to distinguish the phases in the cocontinuous morphology.

The density of the melt blends with dispersed PEO domains increased linearly with PEO content, extrapolating to a value of 1.132 g cm^{-3} for PEO, Figure 3. This value was considerably lower than the measured density of the PEO film of 1.219 g cm^{-3}, and was taken as the density of rubbery, amorphous PEO. A similar value of 1.123 g cm^{-3} has been reported previously for amorphous PEO.[1,18] In contrast, the density of the 50/50 cocontinuous blend which had a crystalline PEO phase fell close to the linear relationship obtained from the measured density of the compression-molded PEO film.

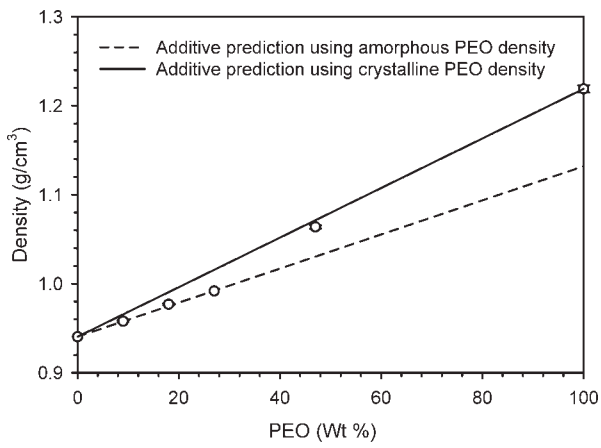

Figure 3 Density of EAA/PEO compression-molded blends as a function of composition. The wt % PEO is extracted from the second DSC heating thermograms.

Gas Permeability of EAA/PEO Blends

The gas permeability through compression molded films was measured at 23°C and 0% RH. The oxygen permeability $P(O_2)$ and the carbon dioxide permeability $P(CO_2)$ are plotted as a function of blend composition in Figure 4. The permeability of 90/10, 80/20, and 70/30 (EAA/PEO) blends increased with the amount of PEO due to the high permeability of the amorphous, rubbery PEO domains.

The blend permeability was compared to predictions of the Maxwell model for a dispersion of spherical particles in a continuous matrix according to[19]

$$\frac{P}{P_{EAA}} = 1 + \frac{3\phi_{PEO}}{\left(\frac{(P_{PEO}/P_{EAA})+2}{(P_{PEO}/P_{EAA})-1}\right) - \phi_{PEO}} \quad (4)$$

where ϕ_{PEO} is the volume fraction PEO in the blend. Equation (4) was fit to the data for the 90/10 and 80/20 blends to obtain P_{aPEO}, the permeability of amorphous PEO. The results with $P_{aPEO}(O_2)$ = 16 barrer and $P_{aPEO}(CO_2)$ = 267 barrer are included as the solid curves in Figure 4(a,b). The O_2 and CO_2 permeabilities of amorphous PEO obtained from the fit to eq. (4) were about 40× higher than the permeabilities of crystallized PEO, which was consistent with the high level of crystallinity achieved in PEO. Because gas transport occurred through the amorphous regions, it followed that the selectivity of 16.7 obtained for amorphous PEO was essentially the same as the selectivity of 16.8 for crystalline PEO.

The permeability of the 70/30 blend fell below the model line because some of the PEO domains had crystallized, not all were amorphous. Eq. (4) as formulated for a dispersion of crystalline PEO domains is included in Figure 4 as a dashed line. Comparison with the solid line for amorphous domains shows

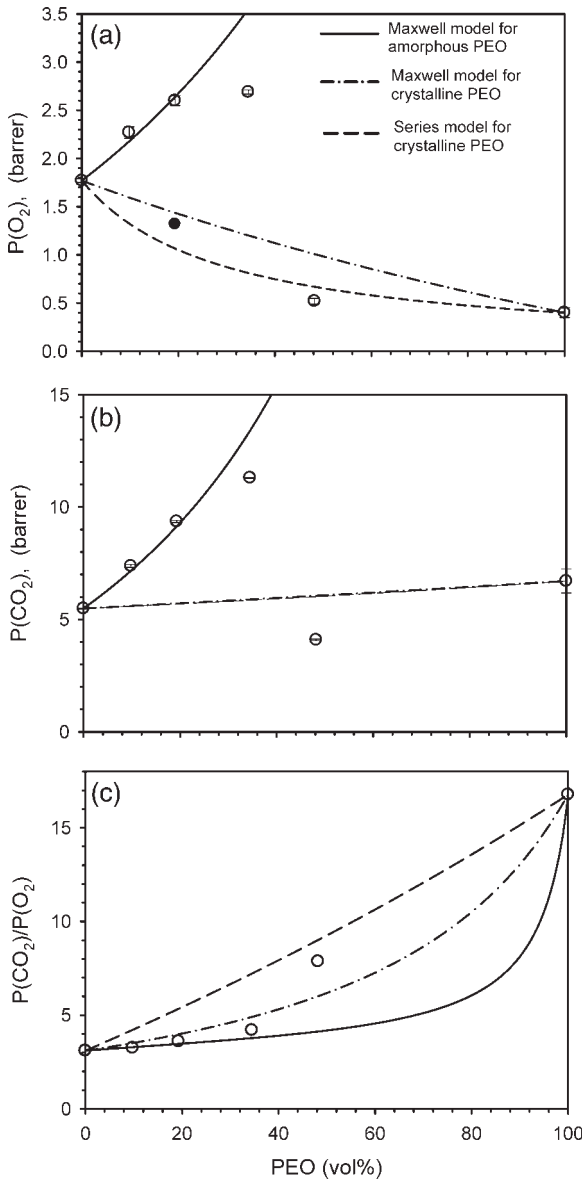

Figure 4 Effect of PEO content on gas permeability of EAA/PEO compression molded blends measured at 23°C and 0% RH: (a) $P(O_2)$; (b) $P(CO_2)$; and (c) $P(CO_2)/P(O_2)$. The result for the 80/20 blend after the PEO domains were crystallized by cooling to −30°C for 5 h is included in (a) as the solid symbol.

the large effect of crystallizing the dispersed domains. This was confirmed by measuring the oxygen permeability of the 80/20 blend after the film was held at −30°C for 5 h to crystallize the PEO domains. The oxygen permeability decreased to 1.32. barrer, which conformed well to eq. (4) for a dispersion of crystalline domains. The data point is included in Figure 4(a) as the solid symbol.

The cocontinuous morphology of the 50/50 blend did not conform to the Maxwell model for dispersed domains as given in Eq. (4). The series model for continuous layers with sharp boundaries which gives P as

$$\frac{1}{P} = \frac{\phi_{PEO}}{P_{PEO}} + \frac{1 - \phi_{PEO}}{P_{EAA}} \tag{5}$$

where ϕ_{PEO} is the volume fraction PEO is included in Figure 4(a). Equation (5) as formulated for crystalline PEO gives a lower bound on the permeability. Although $P(O_2)$ comes close to this prediction, $P(CO_2)$ is lower, which is not readily explained.

At 23°C, the steady state flux was reached very rapidly, so it was not possible to reliably record the nonsteady-state region from which the diffusivity D is conventionally obtained.[10] To obtain D, additional measurements of $P(O_2)$ were performed at 11°C. The oxygen flux curves showed an initial increase which reflected nonsteady-state diffusion, Figure 5. This part of the curve was controlled by the diffusivity D. As the permeant concentration in the specimen reached a constant distribution, the flux reached the steady-state value J_o. The flux curves of EAA and of 90/10, 80/20, and 70/30 (EAA/PEO) blends showed a rapid initial increase in the flux and high steady-state flux. Both the initial slope increased (higher D) and the steady-state flux increased (higher P) with the amount of PEO. In contrast, flux curves of PEO and the 50/50 blend had a longer nonsteady-state region (lower D) and much lower steady-state flux value (lower P).

The oxygen-flux curves were fit to eq. (3). The fit, shown by the solid lines in Figure 5, was equally good for all the experiments in the study. The two fitting parameters P/L and D/L^2 were used to obtain diffusivity D and to accurately determine the permeability P. Solubility S was calculated from $S = PD^{-1}$. For 90/10, 80/20, and 70/30 (EAA/PEO) blends, the increase in P with increasing PEO content was not only due to primarily higher D but also due to a

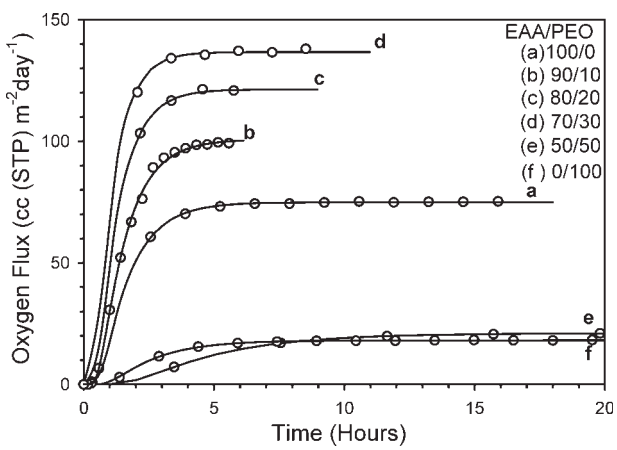

Figure 5 Experimental O_2 flux data for EAA/PEO compression molded blends at 11°C and 0% RH. The data are normalized to a thickness of 625 μm. The solid lines are the fit to eq. (3).

TABLE II
Oxygen Transport Parameters of EAA/PEO Blends at 11°C and 0% RH

Composition EAA/PEO (wt/wt)	Permeability $P(O_2)$ barrer	Diffusivity D $m^2\ s^{-1}$ (10^{-11})	Solubility S cc(STP) $cm^3\ atm^{-1}$
100/0	0.72 ± 0.01	1.05 ± 0.05	0.052 ± 0.002
90/10	0.97	1.13	0.066
80/20	1.17 ± 0.08	1.34 ± 0.02	0.067 ± 0.001
70/30	1.33 ± 0.02	1.65 ± 0.07	0.061 ± 0.002
50/50	0.20	0.35	0.044
0/100	0.18 ± 0.000	0.64 ± 0.03	0.021 ± 0.002

small increase in S, Table II. The large drop in P from 1.33 barrer for the 70/30 blend to 0.20 barrer for the 50/50 blend was due to primarily a decrease in D, with a smaller effect from S. The large decrease in D was attributed to the transition from a dispersed to a cocontinuous PEO phase and to the tortuosity of the diffusion pathway in the PEO phase due to crystallization, whereas the small decrease in S reflected the reduced amorphous phase volume fraction.

Characterization and gas permeability of EAA/PEO microlayers

A representative cross section of a coextruded EAA/PEO multilayer film is shown in Figure 6. All 17 continuous layers are clearly distinguished in the optical micrograph. With the exception of the very thin outer EAA layers, the relative thicknesses of the EAA layers and PEO layers are consistent with the overall 80/20 (EAA/PEO) composition.

Heating thermograms of all the microlayers exhibited a sharp melting peak for PEO at 41°C and a broader melting peak for EAA at 97°C, Figure 7(a).

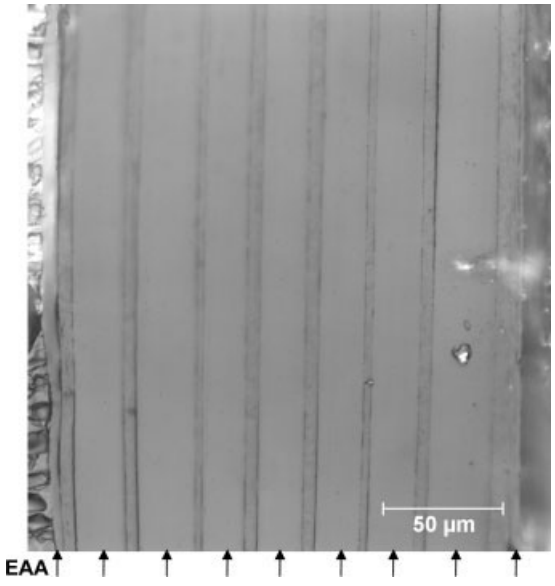

Figure 6 Optical microscope image of the 17-layer 80/20 (EAA/PEO) microlayered film.

Good correspondence was obtained between the measured values of ΔH_m and those calculated from additivity. The cooling thermograms showed crystallization of EAA at 80°C and of PEO at 40°C, Figure 7(b), with ΔH_c values close to those predicted from the composition. The subsequent heating thermograms (not shown) were virtually indistinguishable from the first heating thermograms. The constituent polymers maintained the thermal properties of the bulk in the microns-thick layers.

The density of the microlayer films fell close to the linear relationship obtained from the measured densities of extruded EAA and PEO films, Table III. For subsequent analysis, the microlayer composition (wt/wt) was determined from ΔH_m values in the

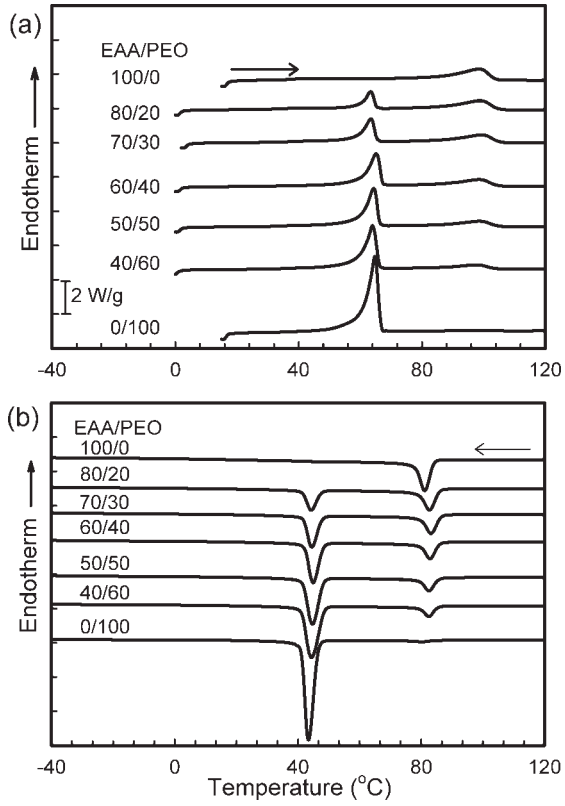

Figure 7 Thermograms of EAA/PEO microlayered films at a heating/cooling rate of 10°C min^{-1}: (a) First heating thermograms beginning at 20°C; and (b) subsequent cooling thermograms.

TABLE III
Composition and Permeability of EAA/PEO Microlayers

Target composition EAA/PEO (vol/vol)	Measured composition from DSC EAA/PEO (wt/wt)	Calculated composition from density EAA/PEO (vol/vol)	Density (g/cm^3)	$P(O_2)$ (barrer)	$P(CO_2)$ (barrer)	$\frac{P(CO_2)}{P(O_2)}$
100/0	100/0	100/0	0.9341 ± 0.0001	2.32 ± 0.16	7.77 ± 0.42	3.7
80/20	79/21	83/17	0.983 ± 0.001	1.44 ± 0.03	7.32 ± 0.35	5.1
70/30	68/32	73/27	1.010 ± 0.002	1.17 ± 0.02	8.21 ± 0.31	7.0
60/40	58/42	64/36	1.035 ± 0.003	1.05 ± 0.01	7.81 ± 0.24	7.4
50/50	51/49	57/43	1.055 ± 0.003	0.81 ± 0.04	7.23 ± 0.23	8.8
40/60	40/60	46/54	1.091 ± 0.001	0.70 ± 0.03	6.89 ± 0.11	9.9
0/100	0/100	0/100	1.203 ± 0.003	0.45 ± 0.01	6.68 ± 0.20	15.1

first DSC heating thermogram. When the composition (vol/vol) was required, the conversion was performed using the measured densities.

The effect of composition on $P(O_2)$ and $P(CO_2)$ of EAA/PEO microlayers is shown in Figure 8. Some variation in the permeability of EAA and PEO between compression molded films and coextruded films (compare Tables I and III) was ascribed to differences in the thermal history. The microlayer composition did not affect $P(CO_2)$ very much because EAA and PEO had similar values. However, PEO had much lower $P(O_2)$ than EAA, and therefore $P(O_2)$ was especially sensitive to the PEO content.

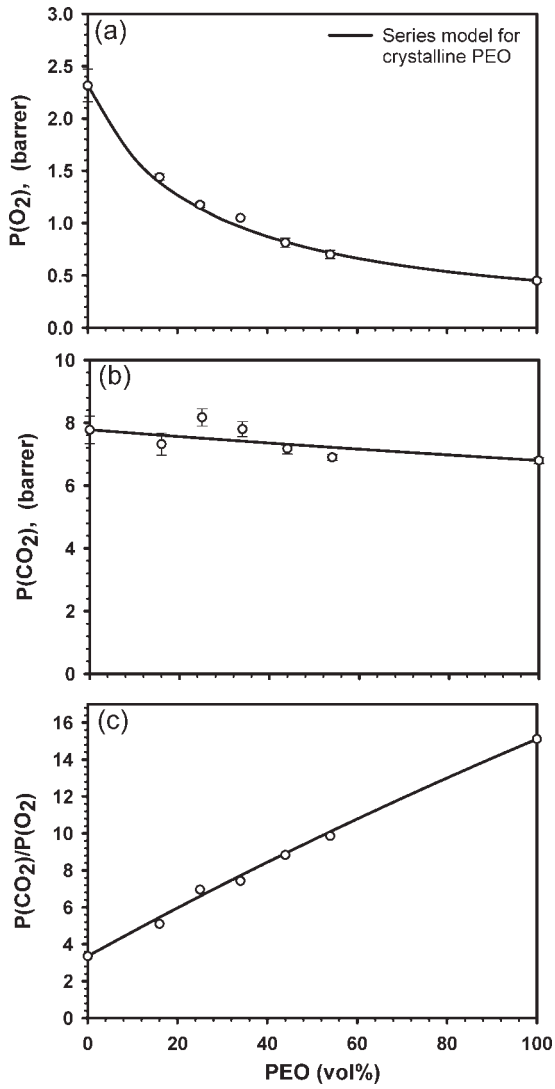

Figure 8 Effect of PEO content on gas permeability of EAA/PEO microlayered films measured at 23°C and 0% RH: (a) $P(O_2)$; (b) $P(CO_2)$; and (c) $P(CO_2)/P(O_2)$.

If the constituent polymers maintained the bulk properties in the layers, as suggested by the thermal behavior, the microlayer structure should conform well to the series model for continuous layers with sharp boundaries and the permeability should be described by eq. (5). Indeed, the oxygen permeability of EAA/PEO microlayers was accurately described by the series model, Figure 8. The high selectivity of PEO was most effectively captured when the PEO phase was continuous as in the microlayers or in the 50/50 blend.

CONCLUSIONS

Polyethylene and PEO are incompatible in melt blends. Introducing about 10 wt % acrylic acid into the polyethylene as an ethylene-acrylic acid copolymer improved the compatibility and resulted in the dispersion of PEO as submicron domains in melt blends, and provided interlayer adhesion of EAA and PEO in coextruded microlayers. Together, the melt blends and coextruded microlayers demonstrated the broad range in gas permeability characteristics that can be achieved with combinations of EAA and PEO. When the PEO was dispersed as small domains, the particles were too numerous for most of them to contain a heterogeneity that was sufficiently active to nucleate crystallization at the normal T_c. The PEO domains remained in the rubbery, amorphous state when the blend was cooled to ambient temperature, and only crystallized at very large undercooling by fractionated crystallization or by homogeneous nucleation. The rubbery, amorphous nature of the PEO domains enhanced the gas permeability of the melt blends. In contrast, the constituent polymers maintained the bulk properties in

5–20 μm-thick microlayers. The series model accurately described the gas transport properties of microlayered films. A comparative study of the $P(CO_2)/P(O_2)$ selectivity ratio in blends and microlayers revealed that the high selectivity of PEO was most effectively captured when the PEO phase was continuous, as in the microlayers or in the cocontinuous 50/50 melt blend.

References

1. Lin, H.; Freeman, B. D. J Membr Sci 2004, 239, 105.
2. Lin, H.; Kai, T.; Freeman, B. D.; Kalakkunnath, S.; Kalika, D. S. Macromolecules 2005, 38, 8381.
3. Lin, H.; Freeman, B. D. J Mol Struct 2005, 739, 57.
4. Halldán, Å.; Wesslén, B. J Appl Polym Sci 1996, 60, 2495.
5. Gonsalves, K. E.; Patel, S. H.; Trivedi, D. H. J Appl Polym Sci 1992, 45, 217.
6. Nuño-Donlucas, S.; Cesteros, L. C.; Puig, J. E.; Katime, I. Macromol Chem Phys 2001, 202, 663.
7. Baer, E.; Kerns, J.; Hiltner, A. In Structure Development During Polymer Processing; Cunha, A. M.; Fakirov; S.; Eds.; Kluwer: Dordrecht, 2000, p 327.
8. Mueller, C.; Kerns, J.; Ebeling, T.; Nazarenko, S.; Hiltner, A.; Baer, E. Polymer Process Engineering; Coates, P. D.; Ed.; The Institute of Materials: London, 1997, p 97, 137.
9. Somlai, L. S.; Liu, R. Y. F.; Landoll, L. M.; Hiltner, A.; Baer, E. J Polym Sci Part B: Polym Phys 2005, 43, 1230.
10. Sekelik, D. J.; Stepanov, S. V.; Nazarenko, S.; Schiraldi, D.; Hiltner, A.; Baer, E. J Polym Sci Part B: Polym Phys 1999, 37, 847.
11. Wunderlich, B. Macromolecular Physics; Academic Press: New York, 1980; Vol. 3, p 42.
12. Kautsky, J. A.; Walton, A. G.; Baer, E. J Appl Phys 1967, 38, 1832.
13. Chen, H. L.; Hsiao, S. C.; Lin, T. L.; Yamauchi, K.; Hasegawa, H.; Hashimoto, T. Macromolecules 2001, 34, 671.
14. Chen, H. L.; Wu, J. C.; Lin, T. L.; Lin, J. S. Macromolecules 2001, 34, 6936.
15. Müller, A. L.; Balsamo, V.; Arnal, T.; Jakob, T.; Schmalz, H.; Abetz, V. Macromolecules 2002, 35, 3048.
16. Massa, M. V.; Carvalho, J. L.; Dalnoki-Veress, K. Eur Phys J E 2003, 12, 111.
17. Mandelkern, L.; Jain, N. L.; Kim H. J Polym Sci Part A-2 1968, 6, 165.
18. Liberman, S. A.; Gomes, A. S.; Macchi, E. M. J Polym Sci: Polym Chem Ed 1984, 22, 2809.
19. Petropoulos, J. H. J Polym Sci Part B: Polym Phys 1985, 23, 1309.